

This is an Open Access document downloaded from ORCA, Cardiff University's institutional repository: <https://orca.cardiff.ac.uk/id/eprint/109932/>

This is the author's version of a work that was submitted to / accepted for publication.

Citation for final published version:

Wang, Qian, Chen, Lifang, Guan, Shaoliang, Zhang, Xin, Wang, Bin, Cao, Xingzhong, Yu, Zhi, He, Yufei, Evans, David G., Feng, Juntong and Li, Dianqing 2018. Ultrathin and vacancy-rich CoAl-layered double hydroxide/graphite oxide catalysts: promotional effect of cobalt vacancies and oxygen vacancies in alcohol oxidation. *ACS Catalysis* 8 , pp. 3104-3115. 10.1021/acscatal.7b03655

Publishers page: <http://dx.doi.org/10.1021/acscatal.7b03655>

Please note:

Changes made as a result of publishing processes such as copy-editing, formatting and page numbers may not be reflected in this version. For the definitive version of this publication, please refer to the published source. You are advised to consult the publisher's version if you wish to cite this paper.

This version is being made available in accordance with publisher policies. See <http://orca.cf.ac.uk/policies.html> for usage policies. Copyright and moral rights for publications made available in ORCA are retained by the copyright holders.



# Ultrathin and Vacancy-Rich CoAl-Layered Double Hydroxide/Graphite Oxide Catalysts: Promotional Effect of Cobalt Vacancies and Oxygen Vacancies in Alcohol Oxidation

Qian Wang,<sup>†,‡</sup> Lifang Chen,<sup>†</sup> Shaoliang Guan,<sup>§</sup> Xin Zhang,<sup>†,‡</sup> Bin Wang,<sup>||</sup> Xingzhong Cao,<sup>⊥</sup> Zhi Yu,<sup>†</sup> Yufei He,<sup>†,‡</sup> David G. Evans,<sup>†</sup> Junting Feng,<sup>\*,†,‡,||</sup> and Dianqing Li<sup>\*,†,‡,||</sup>

<sup>†</sup>State Key Laboratory of Chemical Resource Engineering, Beijing University of Chemical Technology, Beijing 100029, China

<sup>‡</sup>Beijing Engineering Center for Hierarchical Catalysts, Beijing University of Chemical Technology, Beijing 100029, China

<sup>§</sup>Cardi Catalysis Institute, School of Chemistry, Cardiff University, Cardiff, U.K. CF10 3AT

<sup>||</sup>Sinopec Beijing Research Institute of Chemical Industry, Beijing 100013, P. R. China

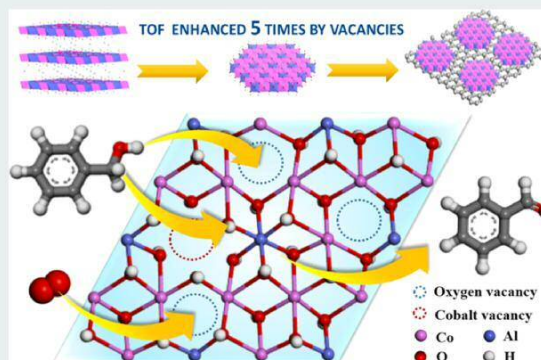
<sup>⊥</sup>Institute of High Energy Physics, Chinese Academy of Sciences, Beijing 100049, China

\* Supporting Information

**ABSTRACT:** Co-containing layered double hydroxides (LDHs) are potential non-noble-metal catalysts for the aerobic oxidation of alcohols. However, the intrinsic activity of bulk LDHs is relatively low. In this work, we fabricated ultrathin and vacancy-rich nanosheets by exfoliating bulk CoAl-LDHs, which were then assembled with graphite oxide (GO) to form a hybrid CoAl-ELDH/GO catalyst. TEM, AFM, and positron annihilation spectrometry indicate that the thickness of the exfoliated LDH platelets is about 3 nm, with a large number of vacancies in the host layers. Fourier transformed XAFS functions show that the Co–O and Co····Co coordination numbers (5.5 and 2.8, respectively) in the hybrid CoAl-ELDH/GO material are significantly lower than the corresponding values in bulk CoAl-LDHs (6.0 and 3.8, respectively). Furthermore, in addition to the oxygen vacancies (VO) and cobalt

vacancies (VCo), CoAl-ELDH/GO also contains negatively charged VCo–Co–OH<sup>δ−</sup> sites and exposed lattice oxygen sites. CoAl-ELDH/GO shows excellent performance as a catalyst for the aerobic oxidation of benzyl alcohol, with a TOF of 1.14 h<sup>−1</sup>; this is nearly five times that of the unexfoliated bulk CoAl-LDHs (0.23 h<sup>−1</sup>) precursor. O<sub>2</sub>-TPD and DRIFT spectroscopy declare that the oxygen storage capacity and mobility are facilitated by the oxygen vacancies and surface lattice oxygen sites. Meanwhile, DFT calculations of adsorption energy show that benzyl alcohol is strongly adsorbed on the oxygen vacancies and negatively charged VCo–Co–OH<sup>δ−</sup> sites. A kinetic isotope effect study further illustrates that the vacancy-rich CoAl-ELDH/GO catalyst accelerates the cleavage of the O–H bond in benzyl alcohol. Finally, we show that the hybrid CoAl-ELDH/GO material exhibits excellent catalytic activity and selectivity in the oxidation of a range of other benzylic and unsaturated alcohols.

**KEYWORDS:** exfoliation, ultrathin, layered double hydroxides, vacancy, selective alcohol oxidation



## 1. INTRODUCTION

Selective aerobic oxidation of primary alcohols using heterogeneous catalysts is an environmentally friendly way to synthesize many organic intermediates. Although much of the earlier effort focused on noble metal catalysts,<sup>1–5</sup> the demand for a sustainable chemical industry requires their replacement by a affordable and abundant non-noble-metal catalysts. Co-based catalysts (mainly cobalt oxides) have been demonstrated to be efficient catalysts for the oxidation of a range of species, including CO,<sup>6,7</sup> CH<sub>4</sub>,<sup>8</sup> VOCs,<sup>9</sup> and olefins.<sup>10</sup> Although some Co-based catalysts have been reported to exhibit high conversion in the oxidation of alcohols, these normally have a high loading of poorly dispersed Co species, thus resulting in low TOF values.<sup>11,12</sup> Therefore, increasing the dispersion of Co species at high loading densities is a key requirement in order

to enhance the activity of Co-based catalysts. Furthermore, the introduction of basic additives as a promoter to facilitate the cleavage of the alcohol O–H bond is also a common route to improve the activity of aerobic alcohol oxidation catalysts.<sup>13,14</sup> Consequently, a material which simultaneously possesses highly dispersed Co species and abundant basic sites could be a promising catalyst for the aerobic oxidation of alcohols.

Layered double hydroxides (LDHs), with the general stoichiometry [M<sup>2+</sup><sub>1–x</sub>M<sup>3+</sup><sub>x</sub>(OH)<sub>2</sub>]<sup>x+</sup>(A<sub>n</sub>)<sub>x/n</sub>·mH<sub>2</sub>O, are a class of 2D layered materials comprising positively charged layers of edge-sharing MO<sub>6</sub> octahedra with charge compensating anions



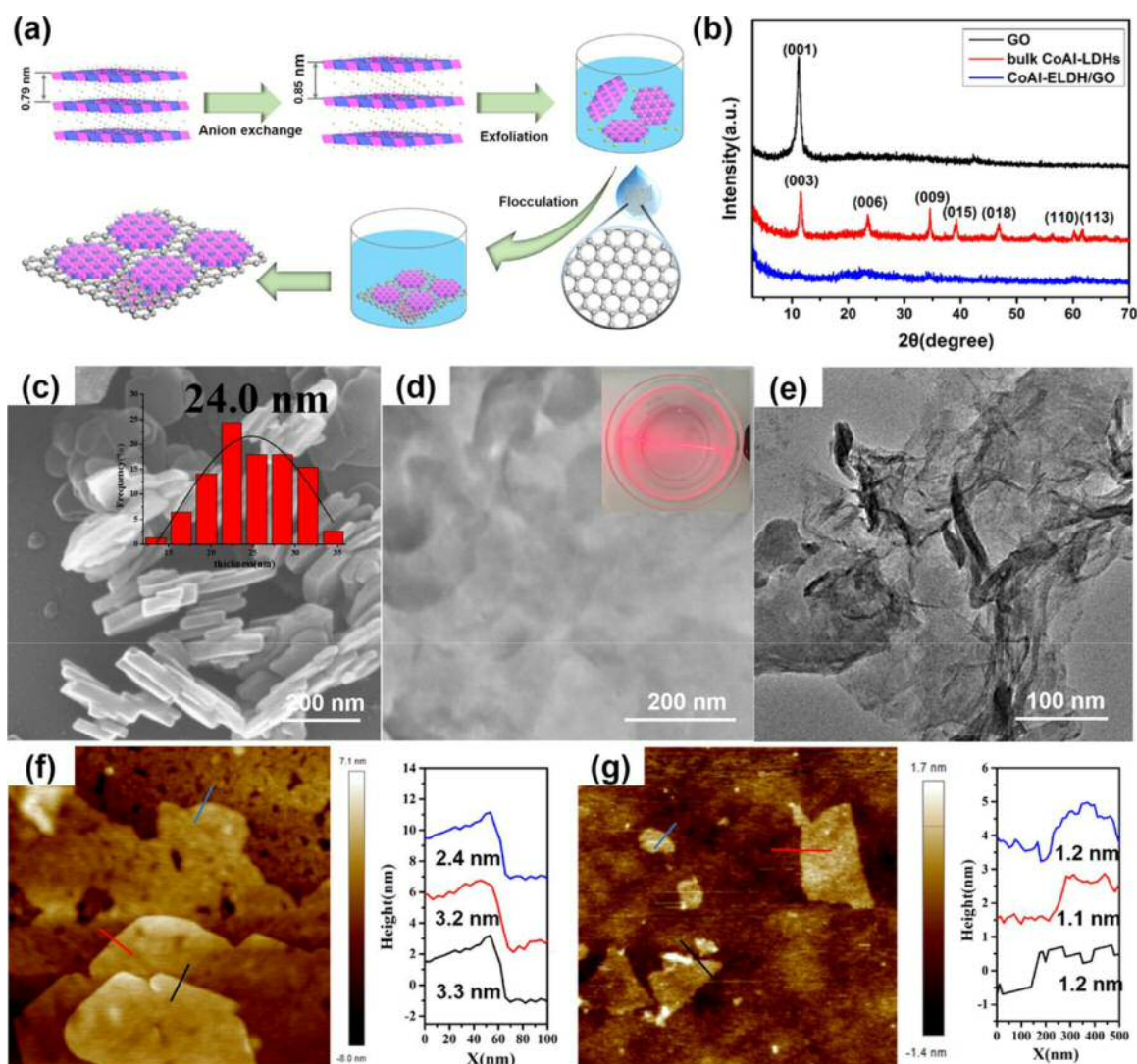


Figure 1. (a) Procedure for heteroassembly of CoAl-LDH nanosheets and GO. (b) XRD patterns of precursors and product. (c) SEM image of bulk CoAl-LDHs and the thickness profile. (d) TEM image of CoAl-ELDHD nanosheets. Inset is a photograph of the Tyndall effect observed when the CoAl-ELDHD solution is irradiated with a laser beam. (e) TEM image of the mechanically exfoliated CoAl-ELDHD nanosheets and their height profiles. (f) AFM image of the ultrasonically exfoliated GO nanosheets and their height profiles. (g) AFM image of the ultrasonically exfoliated GO nanosheets and their height profiles.

between the interlayers.<sup>15</sup> On the basis of the atomic-level dispersion of cations within the brucite-like layer,<sup>16</sup> incorporating both catalytically active and inert metal cations in the layers can result in the high dispersion of active metals in LDH-derived catalysts.<sup>17, 18</sup> In addition, LDHs are well-known heterogeneous solid base catalysts due to the abundance of hydroxyl groups, which can act as Brønsted-type basic sites.<sup>19</sup> These two features of LDHs suggest they are attractive precursors to catalysts with uniformly dispersed Co centers and an abundance of hydroxyl groups.

It has been widely proposed that reducing the thickness of bulk layered materials to ultrathin dimensions, or even to single layers, can alter the intrinsic properties of the materials and enhance their performance as electrocatalysts and photocatalysts.<sup>20,21</sup> In this work, we have synthesized highly crystalline CoAl-LDHs and exfoliated this precursor to a *ord* ultrathin LDH nanosheets using the well-known formamide method.<sup>22</sup> Graphene oxide (GO) was used as a support for the immobilization of the exfoliated LDHs (ELDHD) nanosheets, resulting in a heterogeneous ELDHD/GO nanohybrid.<sup>23</sup> Using benzyl alcohol oxidation as a probe reaction, we compare the

catalytic activities of CoAl-ELDHD/GO and the unexfoliated bulk CoAl-LDHs precursor and show how the presence of abundant vacancies of different types in the former material is responsible for its significantly enhanced catalytic activity.

## 2. RESULTS AND DISCUSSION

**2.1. Structural and Morphological Characterization.** As shown in Figure 1a, the synthesis of CoAl-ELDHD/GO involves the anion-exchange of a carbonate-intercalated CoAl-LDH precursor with nitrate anions, followed by exfoliation of the resulting material in formamide and, finally, combination with an ultrasonically exfoliated suspension of GO. XRD, SEM, TEM, and AFM data for the product are shown in Figure 1 (panels b–g). The XRD pattern of the CoAl-ELDHD/GO nanohybrid (Figure 1c) exhibits greatly reduced intensities of the characteristic peaks<sup>24</sup> for LDHs and GO, which is powerful evidence for successful interlamellar exfoliation. The SEM image in Figure 1c shows that average thickness of bulk CoAl-LDHs platelets is estimated to be 24 nm. After mechanical exfoliation, the suspension of bulk CoAl-LDHs *ords* a

Table 1. Composition of Catalysts and Results of Aerobic Oxidation of Benzyl Alcohol over Various Catalysts<sup>a</sup>

sample	Co:Al (mol:mol) <sup>b</sup>	GO (wt %) <sup>c</sup>	conversion (%)	selectivity (%)				TOF (h <sup>-1</sup> ) <sup>d</sup>
				benzaldehyde	toluene	benzoic acid	benzyl benzoate	
GO	—	—	10.7	91.5	0.1	5.9	2.5	—
bulk CoAl-LDHs	2.6:1	—	37.3	99.1	0	0	0.9	0.23
CoAl-LDHs + GO	2.6:1	15	51.9	92.8	0	6.2	0.9	—
CoAl-ELDHD/GO	1.6:1	15.3	92.2	99.3	0.7	0	0	1.14

<sup>a</sup>Reaction conditions: DMF (5 mL), benzyl alcohol (1 mmol), catalyst (0.015 g for GO and 0.100 g for others), O<sub>2</sub> pressure (1 bar), 120 °C, 4 h.

<sup>b</sup>Determined by ICP. <sup>c</sup>Determined by TG. <sup>d</sup>TOF is based on benzyl alcohol conversion at 0.5 h.

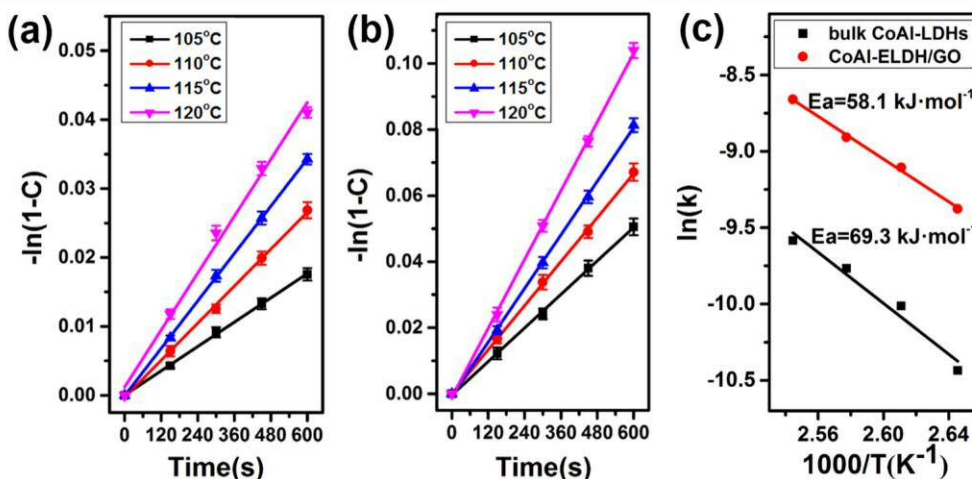


Figure 2. Time-conversion plots at various temperatures for bulk CoAl-LDHs (a), CoAl-ELDHD/GO (b), and Arrhenius plots (c) for benzyl alcohol oxidation. Reaction conditions: DMF (5 mL), benzyl alcohol (1 mmol), catalysts (0.100 g), O<sub>2</sub> pressure (1 bar), 105–120 °C.

transparent pink solution, and the colloidal nature of the solution is confirmed by the clear Tyndall effect observed upon laser irradiation (Figure 1d, inset). A TEM image of the ELDH nanosheets in the colloid (Figure 1d) shows a similar hexagonal sheet morphology to the precursor, but the low contrast confirms the very thin nature of the platelets. The ultrathin character of the exfoliated CoAl-LDH nanosheets is further confirmed by the AFM image shown in Figure 1f, with the height profile shown in the inset. The apparent thickness of the LDH nanosheets is found to be in the range of 2.4–3.3 nm, which suggests the nanosheets consist of only 3 or 4 layers (since the thickness of a single LDH layer is ca. 0.8 nm), as compared with the ca. 30 layers in the unexfoliated precursor. Figure 1g shows an AFM image of the ultrasonically exfoliated GO nanosheets, which have a thickness of 1.1–1.2 nm. The TEM image of the ELDH/GO nanohybrid in Figure 1e confirms that the two types of nanosheets have been incorporated into a hybrid material and shows the high dispersion of the LDH nanosheets.

As shown in Table 1, the Co/Al molar ratio (2.6:1.0) in bulk CoAl-LDHs is close to that in the synthesis mixture (3:1), whereas the ratio in CoAl-ELDHD/GO is only 1.6:1.0, indicating a large number of cobalt vacancies are formed during the mechanical exfoliation process; similar phenomena have been observed after the exfoliation of other bulk materials.<sup>25</sup> The GO content in CoAl-ELDHD/GO was calculated to be 15.3 wt % by TG analysis (Figure S1).

**2.2. Catalytic Performance.** The catalytic performance of CoAl-ELDHD/GO was compared with those of the two precursors and their physical mixture, using benzyl alcohol oxidation as a probe reaction, with DMF as solvent at 120 °C. As shown in Table 1, benzaldehyde is the predominant product

in each case, with small amounts of other products such as benzoic acid, benzyl benzoate, and toluene also being formed. The evolution of the conversion with reaction time is shown in Figure S2. CoAl-ELDHD/GO exhibits significantly higher catalytic activity than those of its precursors, with the conversion of benzyl alcohol after 4 h being approximately three times and nine times those of the values for bulk CoAl-LDHs and pristine GO, respectively. In contrast, the conversion using a physical mixture of GO and bulk CoAl-LDHs is merely that expected from the sum of the values for the separate components, showing that there is no significant synergy obtained simply by mixing the two components. In terms of selectivity, CoAl-LDHs maintains a high selectivity to benzaldehyde of ~99% during the whole reaction, as reported for other LDH-based catalytic systems,<sup>26–28</sup> whereas GO exhibits a lower selectivity of 91.5%, with significant amounts of benzoic acid and benzyl benzoate being formed. The CoAl-ELDHD/GO hybrid material gives the same high selectivity as the LDH precursor, which suggests that the CoAl-LDH nanosheets play the dominant role in hybrid material in terms of both activity and selectivity, and GO mostly acts as a support rather than an active component. The turnover frequency (TOF) was calculated based on the Co species. In accordance with the Co loading (35.51% and 29.16%) and benzyl alcohol conversion at 0.5 h (10.4% and 28.4%), the TOF value for CoAl-ELDHD/GO is five times that of bulk CoAl-LDHs (Table 1). The apparent activation energy ( $E_a$ ) was calculated from Arrhenius plots (Figure 2, panels a–c). The  $E_a$  value for CoAl-ELDHD/GO (58.1 kJ mol<sup>-1</sup>) is much smaller than that for the bulk CoAl-LDHs (69.3 kJ mol<sup>-1</sup>) and is comparable with the previously reported values for a variety of noble metal catalysts.<sup>29–31</sup>

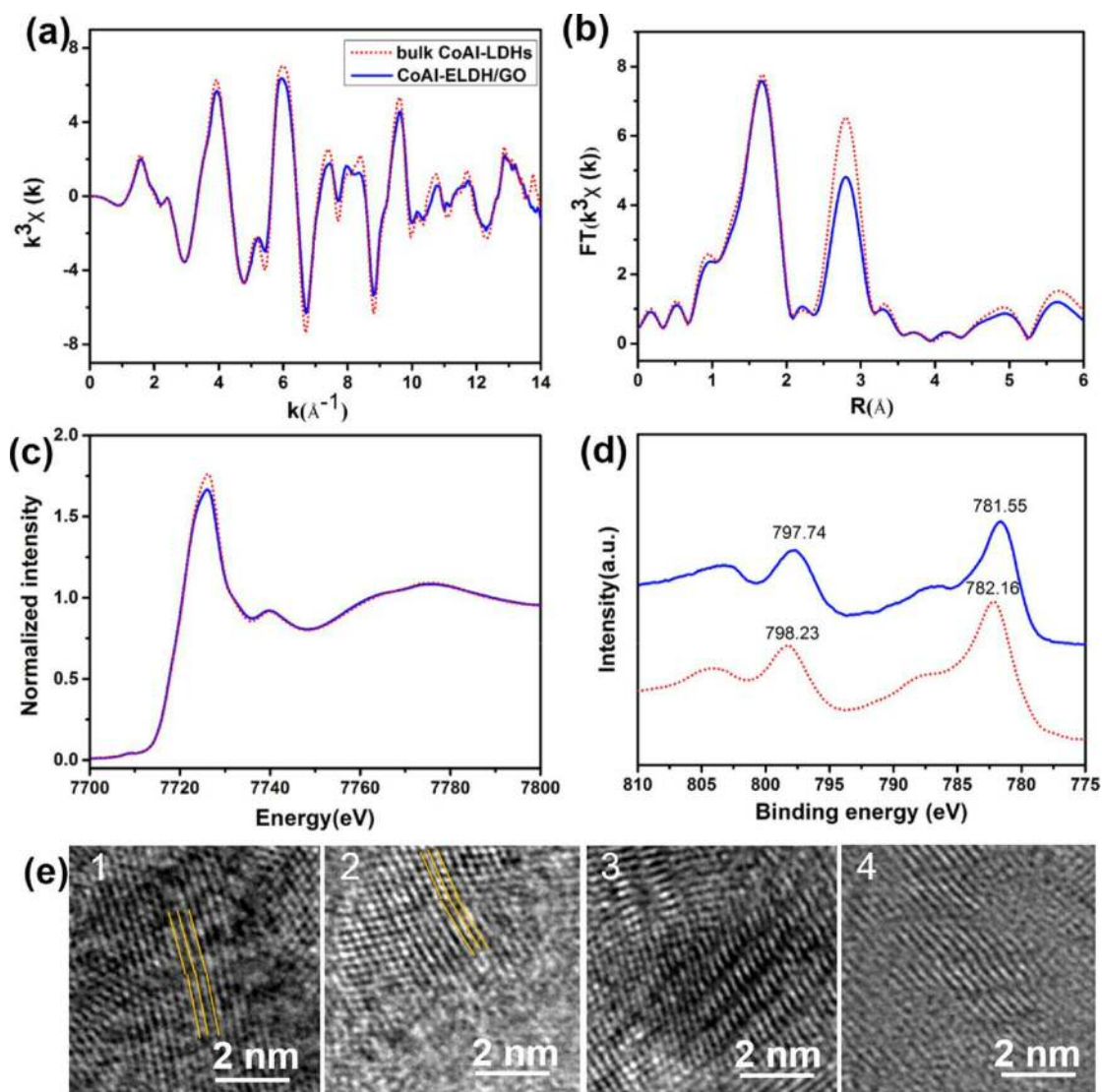


Figure 3. (a) Co K-edge EXAFS  $k^3\chi(k)$  oscillation functions and (b) the corresponding FT curves for CoAl-ELDHO/GO and bulk CoAl-LDHs. (c) The normalized intensity of Co K-edge XANES spectra of CoAl-ELDHO/GO and bulk CoAl-LDHs. (d) XPS spectra of the Co 2p region of CoAl-ELDHO/GO and bulk CoAl-LDHs. (e) The distorted structure of ultrathin CoAl-ELDHO nanosheets.

**2.3. Fine Structure of Catalysts.** Since the analytical data suggest there are a considerable number of Co vacancies in the CoAl-ELDHO/GO catalyst, its surface defects, local atomic arrangement, and electronic structure were investigated in detail. X-ray absorption fine structure spectroscopy (XAFS) was employed to explore the local atomic arrangements in the materials. As shown in Figure 3a, the Co K-edge extended X-ray absorption fine structure spectroscopy (EXAFS)  $k^3\chi(k)$  oscillation curve for CoAl-ELDHO/GO is very similar to that of the bulk LDH, indicating that the ab-plane structure of the host layer is well maintained, which probably results from the protection of the LDH lattice ordered by GO. However, the corresponding Fourier transformed (FT)  $k^3\chi(k)$  functions (Figure 3b) reveal a structural change in the coordination environment of the Co atoms. The FT curves are characterized by two main peaks at 1.6 and 2.8 Å, corresponding to the nearest Co-OOH and next nearest Co····Co coordination, respectively.<sup>32</sup> The peak intensity for Co····Co coordination in CoAl-ELDHO/GO is significantly lower than that for the bulk CoAl-LDHs, while the peak intensity for Co-OOH coordination shows a slight decrease. Fitting of the data for CoAl-LDHs

gives an average Co-OOH distance of 2.09 Å with a coordination number of 6.0 and a Co····Co distance of 3.12 Å with a coordination number of 3.8 (Table S1). For CoAl-ELDHO/GO, although the Co-OOH and Co····Co distances remain essentially unchanged, the Co-OOH and Co····Co coordination numbers decrease significantly to 5.5 and 2.8, respectively, suggesting that the ultrathin nature of the nanosheets results in the formation of coordinatively unsaturated  $\text{CoO}_{6-x}$  octahedra with newly generated cobalt and oxygen vacancies as well as a more distorted structure. Consistent with this, obvious local lattice distortions are visually apparent in HRTEM images (Figure 3e). Such distortions of the atomic arrangement can be expected to result in a change in the electronic structure of CoAl-ELDHO/GO. The differences in the surface atomic structures of the Co centers in the bulk LDHs and the CoAl-ELDHO/GO are apparent from XANES spectra (Figure 3c). Although the normalized Co K-edge XANES spectra of both LDH and ELDHO/GO show an identical photon energy peak at ~7726 eV, the white line intensity for CoAl-ELDHO/GO is lower, confirming the enhanced electron density of Co atoms. The variation in



Table 2. Positron Lifetime Parameters for GO, Bulk CoAl-LDHs, and CoAl-ELDH/GO

sample	$\tau_1$ (ns)	$\tau_2$ (ns)	$\tau_3$ (ns)	$I_1$ (%)	$I_2$ (%)	$I_3$ (%)
GO	0.1894	0.3931	2.518	35.6	62.9	1.6
bulk CoAl-LDHs	0.1829	0.3629	2.538	36.0	62.6	1.4
CoAl-ELDH/GO	0.1947	0.3897	2.652	43.0	55.3	1.7

electron density can be further confirmed by X-ray photoelectron spectroscopy (XPS) (Figure 3d). The Co 2p spectra of bulk CoAl-LDHs and CoAl-ELDH/GO display the characteristic peaks of Co 2p<sub>3/2</sub> centers at 782.16 and 781.55 eV, respectively, with strong satellite features. The data are consistent with a predominance of surface Co<sup>2+</sup> species, but the shift of the peak for CoAl-ELDH/GO toward lower binding energy (BE) is consistent with an increase in the electron density of the Co<sup>2+</sup> species.

The positron annihilation spectra (PAS) of GO, bulk CoAl-LDHs, and CoAl-ELDH/GO all display three distinct lifetime components ( $\tau_1$ ,  $\tau_2$ , and  $\tau_3$ ) with relative intensities ( $I_1$ ,  $I_2$ , and  $I_3$ ) as listed in Table 2. In each case, the two longest components ( $\tau_2$  and  $\tau_3$ ) can be attributed to the annihilation of orthopositronium atoms formed in large defect clusters and in the large voids present in the sample, respectively. In defect-free materials, the shortest component ( $\tau_1$ ) is generally attributed to the annihilation of free positrons,<sup>33,34</sup> but small vacancies existing in disordered systems can decrease the average electron density, thus resulting in elongation of  $\tau_1$ .<sup>35</sup> GO exhibits similar annihilation lifetimes and relative intensities to the bulk CoAl-LDHs. All three samples have comparable values of  $I_3$ , which indicates that the large voids present in the materials are very similar. However,  $\tau_1$  for CoAl-ELDH/GO (0.1947 ns) is longer than that for the bulk CoAl-LDHs (0.1829 ns), which suggests the presence of a new type of small defects in CoAl-ELDH/GO; this is consistent with the EXAFS results. The longer  $\tau_1$  and increased  $I_1$  values (43.0% for CoAl-ELDH/GO, and 36.0% for bulk CoAl-LDHs) can be attributed to annihilation of positrons trapped in cobalt vacancies, as reported elsewhere.<sup>25</sup> The number of cobalt vacancies in CoAl-ELDH/GO is clearly larger than that in the bulk CoAl-LDHs, indicating the predominance of monovacancies ( $I_1$ ) in CoAl-ELDH/GO.

In addition to the formation of these vacancies in CoAl-ELDH/GO, negatively charged V<sub>Co</sub>-Co-OH<sup>δ-</sup> sites were also generated, and more lattice oxygen atoms became exposed. In order to give more specific insight into the surface structure, CO<sub>2</sub> was employed as a probe molecule since it can interact with surface OH and O<sup>2-</sup> groups. The in situ CO<sub>2</sub>-IR spectra collected after adsorbing CO<sub>2</sub> are shown in Figure 4a. The peaks can be assigned to bicarbonates, bidentate carbonates, and monodentate carbonates (Table S2), which arise from the interaction of CO<sub>2</sub> with OH groups, M-O ion pairs, and surface O<sup>2-</sup> ions, respectively.<sup>36,37</sup> The spectrum for CoAl-ELDH/GO is noticeably more complex than those of CoAl-LDHs and GO, with the presence of several strong peaks characteristic of monodentate carbonate moieties, indicating the generation of new isolated surface O<sup>2-</sup> ions associated with the formation of the various vacancies. The CO<sub>2</sub>-TPD traces are shown in Figure 4b. The area and temperature of the low temperature T<sub>1</sub> (100–160 °C) desorption peak for CoAl-ELDH/GO are significantly higher than the corresponding values for CoAl-LDHs, indicating that the former has a larger number of OH groups and a stronger interaction between CO<sub>2</sub> and -OH. This is consistent with the XANES and XPS results, which indicate that the enhanced electronic density of Co

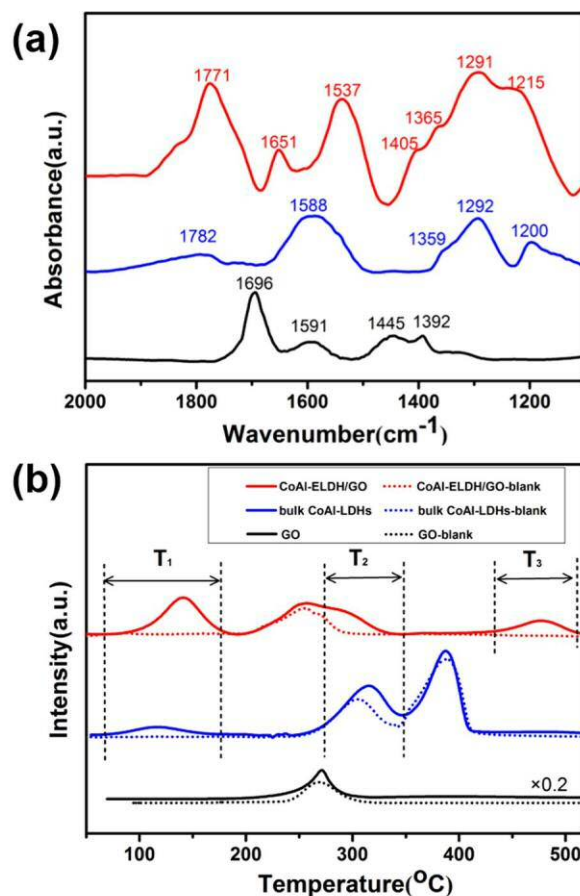


Figure 4. (a) In situ CO<sub>2</sub>-IR spectra and (b) CO<sub>2</sub>-TPD traces for GO, bulk CoAl-LDHs, and CoAl-ELDH/GO.

atoms results in the formation of a larger number of negative Co-OH<sup>δ-</sup> sites in CoAl-ELDH/GO. CoAl-ELDH/GO also shows a peak in the high temperature T<sub>3</sub> region (450–500 °C) which is absent in the trace for CoAl-LDHs; this can be attributed to the presence of surface O<sup>2-</sup> ions, as verified by the in situ CO<sub>2</sub>-IR spectra.

**2.4. Storage and Mobility of Oxygen.** In accordance with the Mars-van Krevelen mechanism,<sup>38</sup> oxygen vacancies and lattice oxygen (O<sup>2-</sup>) can both participate in the storage and mobility of oxygen during oxidation reactions. O<sub>2</sub>-TPD was performed in order to examine the mobility of oxygen species (Figure 5a). Blank tests without adsorbing O<sub>2</sub> were carried to exclude the possibility of decomposition of the samples. For GO, the similar profiles of the blank and O<sub>2</sub>-TPD indicate only very slight adsorption of O<sub>2</sub>. The O<sub>2</sub>-TPD traces of bulk CoAl-LDHs and CoAl-ELDH/GO each have three obvious peaks which, in order of increasing temperature, can be attributed<sup>39,40</sup> to chemisorbed oxygen O<sub>2</sub><sup>-</sup>, active oxygen O<sub>2</sub><sup>2-</sup>, and lattice oxygen O<sub>2</sub><sup>-</sup>.<sup>39,40</sup> The temperatures of the peak maxima are 175, 600, and 810 °C for bulk CoAl-LDHs and 180, 530, and 600 °C for CoAl-ELDH/GO. The temperatures of the peak maxima associated with O<sub>2</sub><sup>2-</sup> and O<sup>2-</sup> are lower for CoAl-ELDH/GO

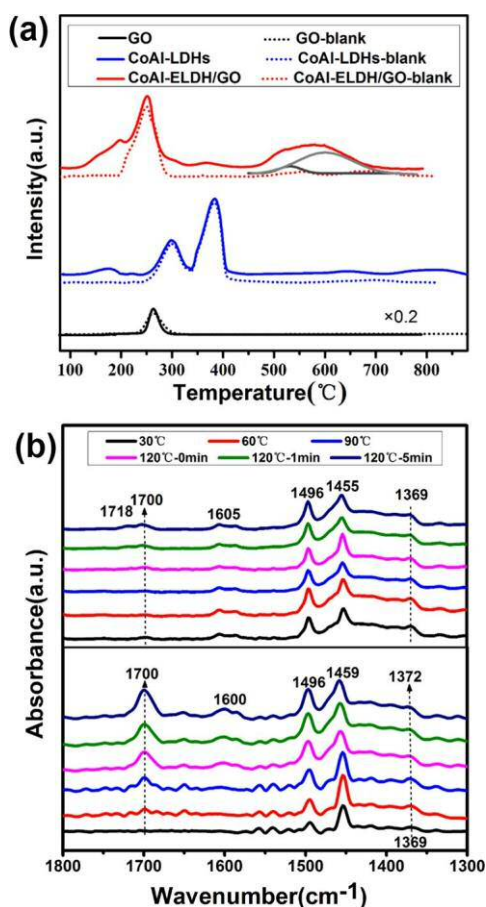


Figure 5. (a) O<sub>2</sub>-TPD traces of GO, bulk CoAl-LDHs, and CoAl-ELDHD/GO samples. (b) DRIFT spectra of benzyl alcohol-dosed bulk CoAl-LDHs (top) and CoAl-ELDHD/GO (bottom).

than the corresponding values for CoAl-LDHs, which indicates a higher oxygen mobility in the former, and can be attributed to the large number of newly generated oxygen vacancies and surface O<sup>2-</sup> ions. Additionally, all of the peaks for CoAl-ELDHD/GO are larger than the corresponding ones for bulk CoAl-LDHs, indicating the increased oxygen adsorption and storage capacity of the former.

DRIFT spectra of benzyl alcohol adsorbed on CoAl-LDHs and CoAl-ELDHD/GO were also recorded (Figure 5b). The weak peak at 1369 cm<sup>-1</sup> can be attributed to the O-H in-plane deformation mode of benzyl alcohol. The intense band associated with aromatic  $\delta$ (C-C) and  $\nu$ (C-H) modes is observed at 1455 cm<sup>-1</sup> for benzyl alcohol adsorbed on bulk CoAl-LDHs and is blue-shifted to 1459 cm<sup>-1</sup> in the case of CoAl-ELDHD/GO, which may be a result of a  $\pi$ - $\pi$  interaction between GO and the benzene ring of benzyl alcohol. Benzaldehyde formation in the proximity of the surface is monitored by the appearance of sharp bands at 1700 and 1718 cm<sup>-1</sup> characteristic of the  $\nu$ (C=O) carbonyl stretch mode of the aldehyde.<sup>41,42</sup> After pretreatment for 1 h under an O<sub>2</sub> atmosphere at the reaction temperature, followed by dosing with small quantities of benzyl alcohol at room temperature, the catalytic behavior was monitored during rapid heating under a He atmosphere. Under these conditions, CoAl-ELDHD/GO gives a significantly higher amount of benzaldehyde than the bulk CoAl-LDHs, suggesting that the presence of more active O<sub>2</sub><sup>2-</sup> associated with newly generated oxygen vacancies facilitates the oxygen flux. Interestingly, a small blue shift is observed from 1369 to 1372 cm<sup>-1</sup> as the temperature is raised, which is probably caused by the enhancement of electron transfer from the hydroxyl group of benzyl alcohol to the catalyst.

## 2.5. Adsorption and Activation of Benzyl Alcohol.

When LDHs are employed as a catalyst or catalyst support in alcohol oxidation, they are generally regarded as solid bases on account of their abundant hydroxyl groups, which are

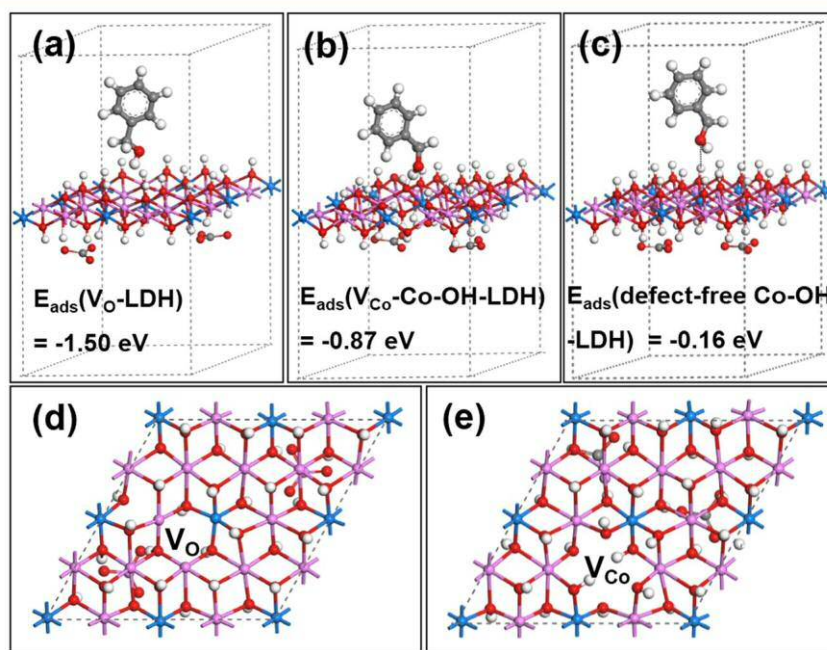


Figure 6. DFT-calculated conformation of adsorption states and adsorption energies of a benzyl alcohol molecule on (a) an oxygen vacancy, (b) a V<sub>Co</sub>-Co-OH<sup>-</sup> site, and (c) defect-free Co-OH. Top views of the optimized structures of (d) an oxygen vacancy and (e) a cobalt vacancy.

considered to act as adsorption sites for alcohols thus facilitating the cleavage of the O–H bond.<sup>26,43–45</sup> However, alcohol adsorption can also occur on oxygen vacancies, as demonstrated by first-principles calculations<sup>46</sup> and experimental studies.<sup>47,48</sup> For example, in the case of selective oxidation of alcohols over an Au/CeO<sub>2</sub> catalyst, Corma et al. found that the Lewis acid sites of the support acted as adsorption sites for alcohols giving a metal alkoxide.<sup>13</sup> In view of the significant differences between the defect structure of bulk CoAl-LDHs and CoAl-ELD/GO, the possible participation of defect-free

Co–OH, Co–OH<sup>δ−</sup> adjacent to Co vacancies (V<sub>Co</sub>–Co–OH<sup>δ−</sup>), oxygen vacancies (V<sub>O</sub>), and cobalt vacancies (V<sub>Co</sub>) in LDHs was investigated. DFT calculations were employed to elucidate the conformation of adsorption states and adsorption energies (E<sub>ads</sub>) of benzyl alcohol on the above sites. The three stable adsorption states are shown in Figure 6. Benzyl alcohol can interact with V<sub>O</sub> through electrostatic attractions and can be hydrogen bonded with defect-free Co–OH and V<sub>Co</sub>–Co–OH<sup>δ−</sup>. The calculated O@benzyl alcohol–H@V<sub>Co</sub>–Co–OH<sup>δ−</sup>-LDH bond length is 1.669 Å, whereas the defect-free Co–OH forms a relatively weak hydrogen bond (2.029 Å). The negative value of E<sub>ads</sub> in each case shows that the adsorption of benzyl alcohol is spontaneous and exothermic, and the absolute value of E<sub>ads</sub> decreases in the order of V<sub>O</sub>-LDH > V<sub>Co</sub>–Co–OH<sup>δ−</sup>-LDH > defect-free Co–OH-LDH. The absolute value of E<sub>ads</sub> for the V<sub>Co</sub>–Co–OH<sup>δ−</sup> sites is larger than that for the defect-free Co–OH sites, indicating that benzyl alcohol forms stronger hydrogen bonds with the former sites. It should be noted that adsorption of benzyl alcohol on the isolated V<sub>Co</sub> sites was energetically unfavorable because of an unfavorable charge repulsion interaction, resulting in a tendency for it to be adsorbed on the adjacent Co–OH<sup>δ−</sup> sites. The calculations therefore show that V<sub>O</sub> and V<sub>Co</sub>–Co–OH<sup>δ−</sup> can be considered as the two main sites where an alcohol molecule is adsorbed via its OH group.

Although many mechanistic studies of alcohol oxidation containing accurate reaction profiles indicate that cleavage of the α-C–H bond is the rate-limiting step,<sup>30,45,49–52</sup> O–H bond cleavage is also of great importance since this is involved in the initial activation of the alcohol.<sup>43</sup> In order to compare the initial O–H bond activation steps occurring over different catalysts, a kinetic isotope effect (KIE) study was performed to study the O–H bond cleavage rates by comparing the reactivity of C<sub>6</sub>H<sub>5</sub>CH<sub>2</sub>OD to that of nonlabeled C<sub>6</sub>H<sub>5</sub>CH<sub>2</sub>OH.<sup>45</sup> The parallel rate constants for C<sub>6</sub>H<sub>5</sub>CH<sub>2</sub>OH and C<sub>6</sub>H<sub>5</sub>CH<sub>2</sub>OD reactants were measured at low conversion (<10%) after 10 min. As shown in Figure 7 (panels a and b), the linear relationship between −ln(1 − C) (where C = concentration of benzyl alcohol) and reaction time shows that the reaction is first order with respect to benzyl alcohol, and the values of the KIE ratios k<sub>H</sub>/k<sub>D</sub> indicate that O–H bond cleavage is a kinetically relevant step. The smaller k<sub>H</sub>/k<sub>D</sub> value for CoAl-ELD/GO relative to that for bulk CoAl-LDHs shows that O–H bond cleavage over this material occurs more easily, which is consistent with its enhanced catalytic activity.

**2.6. Proposed Mechanism.** On the basis of the above evidence and previous data in the literature,<sup>13,26,43,44</sup> two possible reaction pathways for the formation of benzaldehyde over CoAl-ELD/GO catalyst can be proposed, as shown in Figure 8. Initially, O<sub>2</sub> is adsorbed on the oxygen vacancies and captures electrons from adjacent Co<sup>2+</sup> ions to give activated O<sup>−</sup> and Co<sup>3+</sup> species. Simultaneously, the benzyl alcohol molecule is adsorbed on an oxygen vacancy (path I) or V<sub>Co</sub>–Co–OH<sup>δ−</sup>

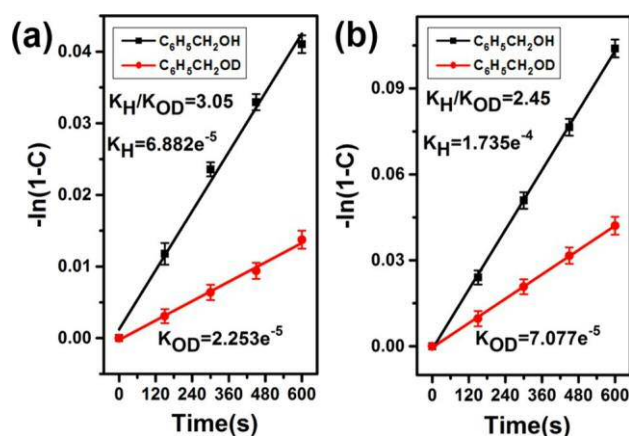


Figure 7. Kinetic isotope effect in the aerobic oxidation of benzyl alcohol and deuterated benzyl alcohol over (a) bulk CoAl-LDHs and (b) CoAl-ELD/GO. Reaction conditions: DMF (5 mL), benzyl alcohol (1 mmol), catalyst (0.100 g), O<sub>2</sub> pressure (1 bar), 120 °C.

(path II), and its O–H group is activated, leading to the abstraction of a proton and the formation of an unstable metal-alkoxide species. This metal-alkoxide species undergoes α-C<sup>δ+</sup>–H<sup>δ−</sup> bond cleavage on an activated O<sup>−</sup> site acting as an H<sup>δ−</sup> acceptor leading to formation of benzaldehyde. Subsequent rapid oxidation of the hydride by activated O<sup>−</sup>, associated with the reduction of Co<sup>3+</sup>–O<sup>−</sup> to Co<sup>2+</sup>–V<sub>O</sub>, followed by desorption of the water molecule from the catalyst completes the catalytic cycle.

**2.7. Recyclability and General Applicability of the Catalysts.** The CoAl-ELD/GO catalyst was reused in six successive reactions, as shown in Figure 9. Although some deactivation was observed over the first four runs, the conversion remained constant at >80% in the following two runs, which is much higher than the conversion even with fresh bulk CoAl-LDHs. The catalytic deactivation is probably due to the agglomeration of a small amount of exfoliated LDH nanosheets which are weakly bound to GO since the XRD pattern (Figure S4a) of the catalyst used six times shows a slightly increased intensity of the (001) basal reflection peaks, indicative of a small degree of restacking of the exfoliated layers. A TEM image (Figure S4a) of the used catalyst shows no significant change in the morphology of the layers themselves, however. XAFS and XPS results (Figures S4, panels c and d) show that the vacancy-rich structure is retained in the reused catalyst. Specifically, the normalized Co K-edge XANES spectra of fresh and used CoAl-ELD/GO show an almost identical white line intensity, indicating that the coordination environment of the Co atoms remains essentially unchanged. In addition, the XPS spectra confirm that the valence state and electron density of Co are also unchanged.

In order to explore the wider applicability of the hybrid CoAl-ELD/GO and bulk CoAl-LDH catalysts, their performance in the selective oxidation of a range of typical alcohols was investigated, and the results are listed in Table 3. CoAl-ELD/GO clearly shows superior catalytic activity to bulk CoAl-LDH in the oxidation of benzylic and unsaturated alcohols. Furthermore, CoAl-ELD/GO shows much higher selectivity for a single product (>94% selectivity in all cases), while bulk CoAl-LDH gives much poorer selectivities in the oxidation of cinnamyl alcohol and phenethyl alcohol despite the much lower conversion. The excellent selectivity shown by CoAl-ELD/GO can be attributed to the presence of a large number of



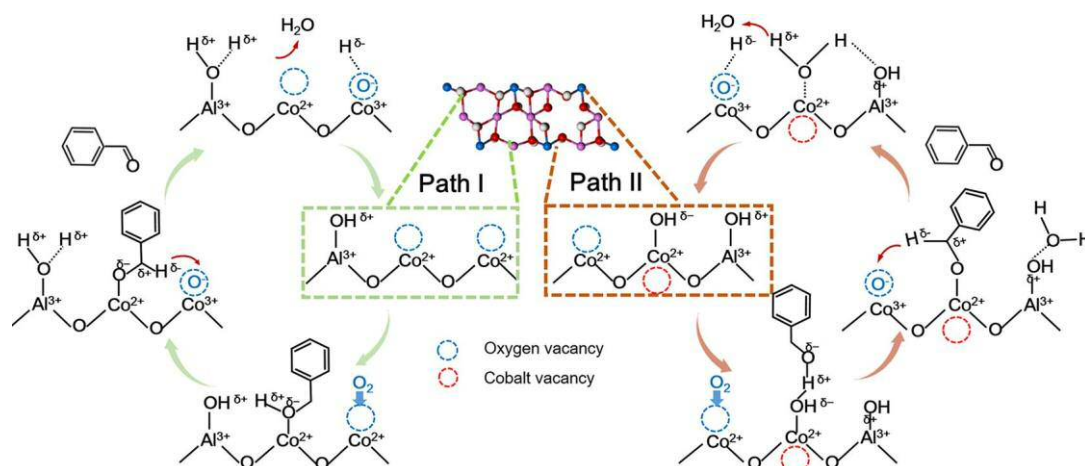


Figure 8. Two possible reaction pathways for the oxidation of benzyl alcohol over the CoAl-ELDHD/GO catalyst.

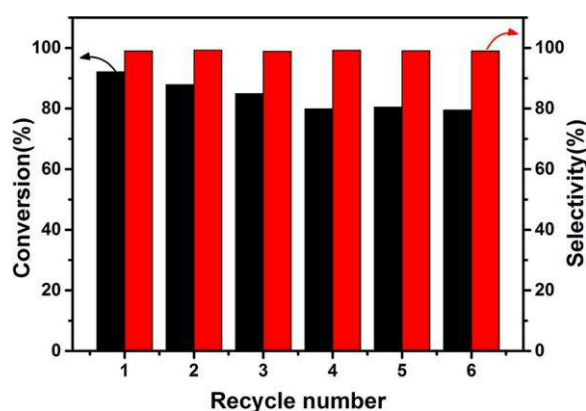


Figure 9. Reusability of the CoAl-ELDHD/GO catalyst.

oxygen vacancies and negatively charged  $V_{Co-Co-OH}^{\delta-}$  sites which facilitate O-H cleavage of alcohols to form the main product. In the case of 1-octanol and cyclohexanol, the extremely low activity of both catalysts can be ascribed to their poor electron donation ability compared with benzylic and unsaturated alcohols, which results in only weak coordination to the active sites.

### 3. CONCLUSION

A hybrid CoAl-ELDHD/GO catalyst can be prepared by coassembly of exfoliated CoAl-LDHs and GO nanosheets. XRD, TEM, and AFM demonstrate that the ultrathin CoAl-ELDHD nanosheets are composed of 3–4 host layers and well-dispersed on the GO support. In the aerobic oxidation of benzyl alcohol, CoAl-ELDHD/GO shows much better catalytic performance than the unexfoliated bulk CoAl-LDHs precursor; the TOF of the former ( $1.14 \text{ h}^{-1}$ ) is nearly five times that of the latter. A kinetic study shows that CoAl-ELDHD/GO possesses much lower  $E_a$  ( $58.1 \text{ kJ mol}^{-1}$ ) than that of bulk CoAl-LDHs ( $69.3 \text{ kJ mol}^{-1}$ ). The ultrathin CoAl-ELDHD/GO catalyst possesses a large number of newly generated cobalt and oxygen vacancies which results in more negatively charged  $V_{Co-Co-OH}^{\delta-}$  sites and exposed lattice oxygen sites. Further studies show that oxygen vacancies and lattice oxygen sites enhance the storage capacity of active  $O_2^{2-}$  and facilitate the oxygen flux. DFT calculations show that the oxygen vacancies and  $V_{Co-Co-OH}^{\delta-}$  are the two most favorable adsorption sites for benzyl alcohol. A kinetic isotope effect study further

indicates that the vacancy-rich CoAl-ELDHD facilitates the cleavage of the alcohol O-H bond and increases the rate of the initial O-H bond activation. These results demonstrate the potential utility of CoAl-ELDHD/GO as an affordable, recyclable, and widely applicable catalyst for selective alcohol oxidation. Furthermore, it should be possible to employ the same synthetic procedure to fabricate a wide range of such hybrid heterogeneous catalysis using other layered materials as precursors.

## 4. EXPERIMENTAL SECTION



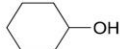
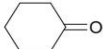
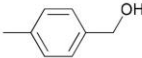
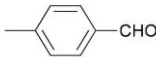
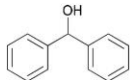
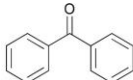
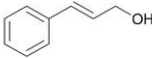
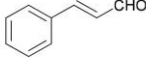
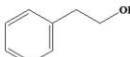
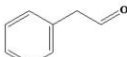
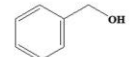
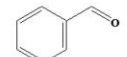
**4.1. Preparation of Catalysts.** The bulk  $CoAl-CO_3^{2-}$ -LDHs precursor was obtained via the urea decomposition method: 0.03 mol of  $Co(NO_3)_2 \cdot 6H_2O$ , 0.01 mol  $Al(NO_3)_3 \cdot 9H_2O$  and as 0.10 mol of urea were dissolved in 70 mL of deionized water, and the solution was aged in a sealed Teflon-lined autoclave at  $150^\circ\text{C}$  for 6 h. The precipitate was separated and washed by centrifugation until the pH of the washings reached 7 and finally dried at  $60^\circ\text{C}$  overnight. Anion exchange was carried out by dispersing 0.3 g of  $CoAl-CO_3^{2-}$ -LDHs into 300 mL of water containing 0.75 M  $NaNO_3$  and 3 mM  $HNO_3$ . The suspension was sealed after purging with nitrogen gas and stirred for 48 h to complete the exchange of the LDH into the form. The exfoliation reaction was carried out by

$NO_3^-$

dispersing 0.3 g of as-synthesized  $CoAl-NO_3$ -LDHs in 300 mL of formamide, the mixture was then sealed after purging with nitrogen gas, and the suspension vigorously stirred for 24 h to obtain a transparent colloid. Graphene oxide (GO) was synthesized using a modified Hummers method. The as-synthesized GO was first dispersed into water and exfoliated by high-power ultrasonication for 30 min to obtained a brown colloidal suspension of GO nanosheets (0.02 g/L). Subsequently, 100 mL of the suspension of GO nanosheets was added drop by drop into 100 mL of the suspension exfoliated  $CoAl-LDHs$  nanosheets (0.1 g/L) with continuous stirring. The flocculated product was stirred for 1 h and then separated by centrifugation and finally dried at  $60^\circ\text{C}$  in a vacuum oven.

**4.2. Catalyst Characterization.** X-ray diffraction (XRD) patterns of the samples were recorded on a Shimadzu XRD-600 X-ray powder diffractometer using a  $Cu K\alpha$  radiation source ( $\lambda = 0.154 \text{ nm}$ ) in the range from  $3^\circ$  to  $70^\circ$  with a scan step of  $10^\circ \text{ min}^{-1}$ . The morphology of the samples was characterized using a Zeiss Supra 55 scanning electron microscope (SEM) and a JEOL JEM-2100F high-resolution transmission electron micro-

Table 3. Aerobic Oxidation of Various Alcohols Using Bulk CoAl-LDHs and CoAl-ELDHDH/GO Catalysts<sup>a</sup>

Entry	Substrate	Main product	Catalyst	Conversion <sup>b</sup> (%)	Selectivity <sup>b</sup> (%)	TON <sup>c</sup>
1			CoAl-ELDHDH/GO	4.6	>99	0.09
			bulk CoAl-LDHs	2.6	>99	0.04
2			CoAl-ELDHDH/GO	3.5	>99	0.07
			bulk CoAl-LDHs	2.9	>99	0.06
3			CoAl-ELDHDH/GO	79.4	96.5 <sup>d</sup>	1.59
			bulk CoAl-LDHs	47.7	>99	0.95
4			CoAl-ELDHDH/GO	25.4	>99	0.51
			bulk CoAl-LDHs	15.2	>99	0.25
5			CoAl-ELDHDH/GO	60.8	94.0 <sup>e</sup>	1.21
			bulk CoAl-LDHs	25.0	72.7 <sup>e</sup>	0.50
6			CoAl-ELDHDH/GO	49.7	98.3 <sup>f</sup>	0.99
			bulk CoAl-LDHs	10.7	86.2 <sup>f</sup>	0.21
7			CoAl-ELDHDH/GO	92.2	>99	1.86
			bulk CoAl-LDHs	37.3	>99	0.62

<sup>a</sup>Reaction conditions: DMF (5 mL), alcohol (1 mmol), catalyst (0.100 g), O<sub>2</sub> pressure (1 bar), 120 °C, 4 h. <sup>b</sup>The products are determined by GC/MS analysis, and conversion and selectivity are determined by GC via an internal standard technique with carbon balance within 100 ± 5%.

<sup>c</sup>Turnover number given in mol<sub>alcohol</sub> · mol<sub>total Co</sub><sup>-1</sup> is based on the conversion at 4 h. <sup>d</sup>Byproduct: p-toluylic acid. <sup>e</sup>Byproduct: 3-phenyl-1-propanol.

<sup>f</sup>Byproduct: phenylacetic acid

scope (HRTEM). The thickness of the exfoliated CoAl-LDH nanosheets was estimated using a Digital Instruments Version 6.12 atomic force microscope (AFM). Thermal analysis was performed on a TG/DTA X70 thermogravimetric analyzer in air by ramping the temperature from 30 to 700 °C with a heating rate of 10 °C min<sup>-1</sup>. Metal content was measured using a Shimadzu ICPS-75000 inductively coupled plasma emission spectrometer (ICP-AES). The Co K-edge XANES measurements were performed at beamline 1W1B of the Beijing Synchrotron Radiation Facility (BSRF). The X-ray photo-electron spectroscopy (XPS) spectra were collected using a Thermo VG ESCALAB 250 spectrometer equipped with an Al K $\alpha$  anode, with the calibration peak being the C 1s peak at 284.6 eV. Positron annihilation experiments (PAS) using a sandwiched sample/<sup>22</sup>Na source/sample were performed on a fast-slow coincidence ORTEC system with a time resolution of 195 ps full width at half-maximum, and positron lifetime calculations were carried out using the LT9.0 software. Temperature-programmed desorption (TPD) was performed on a Micromeritics Chemisorb 2750 chemisorption instrument with a thermal conductivity detector (TCD). The sample (0.1000 g) was preheated at 120 °C for 1 h in He flow (99.9%), followed by cooling to room temperature. The sample was then kept in a stream of CO<sub>2</sub> for 1 h to ensure the adsorption was saturated, and the sample was then purged with He flow for

another 1 h. The CO<sub>2</sub>-TPD curve was collected by ramping the temperature from 30 to 600 °C with He as a carrier gas (40 mL/min). The pretreatment for O<sub>2</sub>-TPD samples was the same as for CO<sub>2</sub>-TPD except that the adsorption gas was 5% oxygen/ helium. The O<sub>2</sub>-TPD curve was collected by ramping the temperature from 30 to 950 °C with He as carrier gas (40 mL/min). Di use reflectance Fourier transform infrared (DRIFT) spectra were recorded on a Bruker Tensor 27 spectrometer installed with a highly sensitive MCT detector and a di use IR heating chamber equipped with KBr windows. For the in situ CO<sub>2</sub> DRIFT measurements, the sample was pretreated at 120 °C for 1 h in a N<sub>2</sub> flow. After an initial scan as the background spectrum, CO<sub>2</sub> was then passed over the sample for 1 h. After purging with N<sub>2</sub> for a few minutes to remove CO<sub>2</sub>, spectra were collected in the range 2000–1000 cm<sup>-1</sup> with 64 accumulation scans at room temperature and a pressure less than 10<sup>-3</sup> Pa. For in situ benzyl alcohol DRIFT measurements, after identical pretreatment and background spectra collection, the temperature was raised to 120 °C and O<sub>2</sub> was passed over the sample for 1 h. Then the sample was cooled down and a small amount of benzyl alcohol was passed over the sample for 1 h using an in-line saturator. Subsequently, the spectra were collected in the range of 4000–400 cm<sup>-1</sup> with 64 accumulation scans at temperatures in the range from 30 to 120 °C with a ramping rate of 10 °C/min.

**4.3. Benzyl Alcohol Oxidation.** The liquid-phase oxidation of benzyl alcohol was performed in a 50 mL quartz reactor. Prior to reaction, catalyst (0.015 g for GO and 0.100 g for others), 1 mmol benzyl alcohol, and 5 mL of N,N-dimethylformamide (DMF) were added to the reactor. Prior to reaction, the system was purged with O<sub>2</sub> several times to remove air, and then the sealed reactor was kept in a heating block which was preheated to the reaction temperature, and the relative pressure of O<sub>2</sub> was elevated to 1 bar. The mixture was stirred using a magnetic bar with a high speed of 1000 rpm. After a specific reaction time, the reactor was held in an ice bath until the reaction mixture was cooled, and then the liquid and solid catalyst were separated by centrifugation. The catalyst was sequentially washed three times with acetone and once with 0.1 M NaOH solution and then washed with deionized water until the pH reached 7. After drying at 60 °C for 10 h, the catalyst was reused in a second run under the same conditions. Finally, the reaction mixture (1 mL of reaction products with 0.1 mL of dodecane as external standard) was analyzed using a Agilent J&W gas chromatograph equipped with a FID detector and a DB-WAX capillary column (30 m × 0.320 mm, d<sub>f</sub> = 0.25 μm). The reaction products were identified by comparison with known standards. In all cases, the carbon balances were 100 ± 5%.

The kinetic isotope effect study was performed by measuring the reaction rates for 10 min, using C<sub>6</sub>H<sub>5</sub>CH<sub>2</sub>OH and C<sub>6</sub>H<sub>5</sub>CH<sub>2</sub>OD as substrates. The deuterated benzyl alcohol-OD was prepared according to the literature: 0.75 g of NaH was added to a Schlenk flask which was charged with a N<sub>2</sub> atmosphere, and then 3.0 g of benzyl alcohol and 50 mL of dry tetrahydrofuran were added. After stirring at room temperature for 1 h, 3 equiv. (0.83 g) of D<sub>2</sub>O (99.9 atom % D) was added to the suspension. The deuterated benzyl alcohol-OD was extracted three times with dry diethyl ether, and the combined organic phase was dried over Na<sub>2</sub>SO<sub>4</sub>. The solvent was removed in vacuo to afford C<sub>6</sub>H<sub>5</sub>CH<sub>2</sub>OD (confirmed by <sup>1</sup>H NMR, Figure S5).

**4.4. Computational Methods.** Density functional theory (DFT) calculations were performed using the DMol<sup>53,54</sup>

<sup>53,54</sup> module in the Material Studio 7.0 software package

(Accelrys Software Inc., San Diego, CA).<sup>53,55</sup> The unit cell structural models for LDH were built according to the experimental data. The generalized gradient approximation (GGA) with the Perdew–Burke–Ernzerhof (PBE)<sup>56</sup> functional, together with an orbital cutoff of 4.2 Å and a double-numerical plus polarization (DNP) basis set were utilized for all the calculations. Effective core potentials were used to treat the core electrons of cobalt. The k-points were set at 3 × 3 × 1 in calculating the electronic structures, with spin-polarized Hubbard DFT+U<sup>57</sup> added for all optimizations, where the value of U is 3.52 eV for Co.<sup>58</sup> A Fermi smearing of 0.01 Ha was used to ensure the fast convergence of the self-consistent field iterations.<sup>59</sup> A 4 × 4 × 1 supercell was adopted for the LDH material. Two carbonate anions were introduced into the interlayer space to keep the system neutral. The vacuum was set to be 20 Å in the z direction to minimize the interaction between neighboring slabs. The convergence criteria for the geometry optimizations were 1 × 10<sup>−4</sup> Ha/atom for energy and 0.02 Ha/Å for force, and the displacement was 0.05 Å. The self-consistent field (SCF) convergence criterion was 1 × 10<sup>−4</sup> Ha. The adsorption energies (E<sub>ads</sub>) of the reactants and products were calculated according to the equation

$$E_{\text{ads}} = E_{\text{total}} - E_{\text{adsorbate}} - E_{\text{surf}} \quad (1)$$

where E<sub>total</sub> is the energy of the system after adsorption, E<sub>surf</sub> is the energy of the surface before adsorption (clean surface), and E<sub>adsorbate</sub> is the energy of the free adsorbate in the gas phase. Therefore, larger adsorption energies (absolute value) correspond to stronger adsorption.

## ■ ASSOCIATED CONTENT

### \* Supporting Information

Thermogravimetric profiles of the catalysts, evolution of the conversion with reaction time over different catalysts, EXAFS curve-fitting results for the bulk CoAl-LDHs and CoAl-ELD/GO, XRD patterns of fresh and used CoAl-ELD/GO catalyst, and <sup>1</sup>H NMR spectra of C<sub>6</sub>H<sub>5</sub>CH<sub>2</sub>OH and C<sub>6</sub>H<sub>5</sub>CH<sub>2</sub>OD (Figures S1–S5) and local structure parameters around Co estimated by EXAFS analysis and carbonate mode assignment from CO<sub>2</sub> adsorption and desorption (Tables S1–S2) (PDF)

## ■ AUTHOR INFORMATION

### Corresponding Authors

\*Address: Box 98, 15 Bei San Huan East Road, Beijing 100029, China. Tel: +86 10 64436992. Fax: +86 10 64436992. E-mail: fengjt@mail.buct.edu.cn.

\*E-mail: lidq@mail.buct.edu.cn.

### ORCID

Xin Zhang: 0000-0003-3559-2096

Xingzhong Cao: 0000-0001-5011-5912

Junting Feng: 0000-0002-6211-9651

Dianqing Li: 0000-0001-6761-8946

### Notes

The authors declare no competing financial interest.

## ■ ACKNOWLEDGMENTS

This work was supported by National Natural Science Foundation (21576021 and 2152100), National Key Research and Development Program of China (2017YFA0206804), and the Fundamental Research Funds for the Central Universities (BHYC1701B and JD1816).

## ■ REFERENCES

- (1) Corma, A.; Garcia, H. Supported Gold Nanoparticles as Catalysts for Organic Reactions. *Chem. Soc. Rev.* 2008, 37, 2096–2126.
- (2) Mori, K.; Hara, T.; Mizugaki, T.; Ebitani, K.; Kaneda, K. Hydroxyapatite-Supported Palladium Nanoclusters: A Highly Active Heterogeneous Catalyst for Selective Oxidation of Alcohols by Use of Molecular Oxygen. *J. Am. Chem. Soc.* 2004, 126, 10657–10666.
- (3) Mallat, T.; Bodnar, Z.; Hug, P.; Baiker, A. Selective Oxidation of Cinnamyl Alcohol to Cinnamaldehyde with Air over Bi-Pt/Alumina Catalysts. *J. Catal.* 1995, 153, 131–143.
- (4) Mallat, T.; Baiker, A. Oxidation of Alcohols with Molecular Oxygen on Solid Catalysts. *Chem. Rev.* 2004, 104, 3037–3058.
- (5) Zhan, B.; White, M. A.; Sham, T. K.; Pincock, J. A.; Doucet, R. J.; Rao, K. R.; Robertson, K. N.; Cameron, T. S. Zeolite-Confined Nano-RuO<sub>2</sub>: A Green, Selective, and Efficient Catalyst for Aerobic Alcohol Oxidation. *J. Am. Chem. Soc.* 2003, 125, 2195–2199.
- (6) Xie, X.; Li, Y.; Liu, Z.; Haruta, M.; Shen, W. Low-Temperature Oxidation of CO Catalysed by Co<sub>3</sub>O<sub>4</sub> Nanorods. *Nature* 2009, 458, 746–749.



- (7) Jones, C.; Taylor, S. H.; Burrows, A.; Crudace, M. J.; Kiely, C. J.; Hutchings, G. J. Cobalt Promoted Copper Manganese Oxide Catalysts for Ambient Temperature Carbon Monoxide Oxidation. *Chem. Commun.* 2008, 1707–1709.
- (8) Hu, L.; Peng, Q.; Li, Y. Selective Synthesis of Co<sub>3</sub>O<sub>4</sub> Nanocrystal with Different Shape and Crystal Plane Effect on Catalytic Property for Methane Combustion. *J. Am. Chem. Soc.* 2008, 130, 16136–16137.
- (9) Nguyen, H.; El-Safty, S. A. Meso- and Macroporous Co<sub>3</sub>O<sub>4</sub> Nanorods for Effective VOC Gas Sensors. *J. Phys. Chem. C* 2011, 115, 8466–8474.
- (10) Ma, C. Y.; Mu, Z.; Li, J. J.; Jin, Y. G.; Cheng, J.; Lu, G. Q.; Hao, Z. P.; Qiao, S. Z. Mesoporous Co<sub>3</sub>O<sub>4</sub> and Au/Co<sub>3</sub>O<sub>4</sub> Catalysts for Low-Temperature Oxidation of Trace Ethylene. *J. Am. Chem. Soc.* 2010, 132, 2608–2613.
- (11) Nie, R.; Shi, J.; Du, W.; Ning, W.; Hou, Z.; Xiao, F. A Sandwich N-Doped Graphene/Co<sub>3</sub>O<sub>4</sub> Hybrid: An Efficient Catalyst for Selective Oxidation of Olefins and Alcohols. *J. Mater. Chem. A* 2013, 1, 9037–9045.
- (12) Zhu, J.; Kailasam, K.; Fischer, A.; Thomas, A. Supported Cobalt Oxide Nanoparticles as Catalyst for Aerobic Oxidation of Alcohols in Liquid Phase. *ACS Catal.* 2011, 1, 342–347.
- (13) Abad, A.; Concepcion, P.; Corma, A.; Garcia, H. A Collaborative Effect between Gold and a Support Induces the Selective Oxidation of Alcohols. *Angew. Chem., Int. Ed.* 2005, 44, 4066–4069.
- (14) Yang, J.; Guan, Y.; Verhoeven, T.; van Santen, R.; Li, C.; Hensen, E. J. Basic Metal Carbonate Supported Gold Nanoparticles: Enhanced Performance in Aerobic Alcohol Oxidation. *Green Chem.* 2009, 11, 322–325.
- (15) Sideris, P. J.; Nielsen, U. G.; Gan, Z.; Grey, C. P. Mg/Al Ordering in Layered Double Hydroxides Revealed by Multinuclear NMR Spectroscopy. *Science* 2008, 321, 113–117.
- (16) Fan, G.; Li, F.; Evans, D. G.; Duan, X. Catalytic Applications of Layered Double Hydroxides: Recent Advances and Perspectives. *Chem. Soc. Rev.* 2014, 43, 7040–7066.
- (17) Feng, J.; Lin, Y.; Evans, D. G.; Duan, X.; Li, D. Enhanced Metal Dispersion and Hydrodechlorination Properties of a Ni/Al<sub>2</sub>O<sub>3</sub> Catalyst Derived from Layered Double Hydroxides. *J. Catal.* 2009, 266, 351–358.
- (18) Liu, Y.; He, Y.; Zhou, D.; Feng, J.; Li, D. Catalytic Performance of Pd-Promoted Cu Hydrotalcite-Derived Catalysts in Partial Hydro-genation of Acetylene: Effect of Pd–Cu Alloy Formation. *Catal. Sci. Technol.* 2016, 6, 3027–3037.
- (19) Wang, Q.; O'Hare, D. Recent Advances in the Synthesis and Application of Layered Double Hydroxide (LDH) Nanosheets. *Chem. Rev.* 2012, 112, 4124–4155.
- (20) Gunjekar, J. L.; Kim, T. W.; Kim, H. N.; Kim, I. Y.; Hwang, S. J. Mesoporous Layer-by-Layer Ordered Nanohybrids of Layered Double Hydroxide and Layered Metal Oxide: Highly Active Visible Light Photocatalysts with Improved Chemical Stability. *J. Am. Chem. Soc.* 2011, 133, 14998–15007.
- (21) Liu, Y.; Hua, X.; Xiao, C.; Zhou, T.; Huang, P.; Guo, Z.; Pan, B.; Xie, Y. Heterogeneous Spin States in Ultrathin Nanosheets Induce Subtle Lattice Distortion to Trigger Efficient Hydrogen Evolution. *J. Am. Chem. Soc.* 2016, 138, 5087–5092.
- (22) Liu, Z.; Ma, R.; Osada, M.; Iyi, N.; Ebina, Y.; Takada, K.; Sasaki, T. Synthesis, Anion Exchange, and Delamination of Co–Al Layered Double Hydroxide: Assembly of the Exfoliated Nanosheet/Polyanion Composite Films and Magneto-Optical Studies. *J. Am. Chem. Soc.* 2006, 128, 4872–4880.
- (23) Ma, W.; Ma, R.; Wang, C.; Liang, J.; Liu, X.; Zhou, K.; Sasaki, T. A Superlattice of Alternately Stacked Ni–Fe Hydroxide Nanosheets and Graphene for Efficient Splitting of Water. *ACS Nano* 2015, 9, 1977–1984.
- (24) Xu, J.; Gai, S.; He, F.; Niu, N.; Gao, P.; Chen, Y.; Yang, P. A Sandwich-Type Three-Dimensional Layered Double Hydroxide Nanosheet Array/Graphene Composite: Fabrication and High Supercapacitor Performance. *J. Mater. Chem. A* 2014, 2, 1022–1031.
- (25) Liu, Y.; Cheng, H.; Lyu, M.; Fan, S.; Liu, Q.; Zhang, W.; Zhi, Y.; Wang, C.; Xiao, C.; Wei, S.; et al. Low Overpotential in Vacancy-Rich Ultrathin CoSe<sub>2</sub> Nanosheets for Water Oxidation. *J. Am. Chem. Soc.* 2014, 136, 15670–15675.
- (26) Du, Y.; Wang, Q.; Liang, X.; He, Y.; Feng, J.; Li, D. Hydrotalcite-Like MgMnTi Non-Precious-Metal Catalyst for Solvent-Free Selective Oxidation of Alcohols. *J. Catal.* 2015, 331, 154–161.
- (27) Zhou, W.; Tao, Q.; Pan, J.; Liu, J.; Qian, J.; He, M.; Chen, Q. Effect of Basicity on the Catalytic Properties of Ni-Containing Hydrotalcites in the Aerobic Oxidation of Alcohol. *J. Mol. Catal. A: Chem.* 2016, 425, 255–265.
- (28) Choudary, B.; Kantam, M. L.; Rahman, A.; Reddy, C.; Rao, K. K. The First Example of Activation of Molecular Oxygen by Nickel in Ni–Al Hydrotalcite: A Novel Protocol for the Selective Oxidation of Alcohols. *Angew. Chem., Int. Ed.* 2001, 40, 763–766.
- (29) Bavykin, D. V.; Lapkin, A. A.; Kolaczkowski, S. T.; Plucinski, P. K. Selective Oxidation of Alcohols in a Continuous Multifunctional Reactor: Ruthenium Oxide Catalysed Oxidation of Benzyl Alcohol. *Appl. Catal., A* 2005, 288, 175–184.
- (30) Yamaguchi, K.; Mizuno, N. Scope, Kinetics, and Mechanistic Aspects of Aerobic Oxidations Catalyzed by Ruthenium Supported on Alumina. *Chem. - Eur. J.* 2003, 9, 4353–4361.
- (31) Huang, X.; Wang, X.; Wang, X.; Wang, X.; Tan, M.; Ding, W.; Lu, X. P123-Stabilized Au–Ag Alloy Nanoparticles for Kinetics of Aerobic Oxidation of Benzyl Alcohol in Aqueous Solution. *J. Catal.* 2013, 301, 217–226.
- (32) Huang, J.; Chen, J.; Yao, T.; He, J.; Jiang, S.; Sun, Z.; Liu, Q.; Cheng, W.; Hu, F.; Jiang, Y.; et al. CoOOH Nanosheets with High Mass Activity for Water Oxidation. *Angew. Chem.* 2015, 127, 8846–8851.
- (33) Dutta, S.; Chattopadhyay, S.; Jana, D.; Banerjee, A.; Manik, S.; Pradhan, S.; Sutradhar, M.; Sarkar, A. Annealing Effect on Nano-ZnO Powder Studied from Positron Lifetime and Optical Absorption Spectroscopy. *J. Appl. Phys.* 2006, 100, 114328.
- (34) Kong, M.; Li, Y.; Chen, X.; Tian, T.; Fang, P.; Zheng, F.; Zhao, X. Tuning the Relative Concentration Ratio of Bulk Defects to Surface Defects in TiO<sub>2</sub> Nanocrystals Leads to High Photocatalytic Efficiency. *J. Am. Chem. Soc.* 2011, 133, 16414–16417.
- (35) Sanyal, D.; Banerjee, D.; De, U. Probing (Bi<sub>0.92</sub>Pb<sub>0.17</sub>)<sub>2</sub>Sr<sub>1.91</sub>Ca<sub>2.03</sub>Cu<sub>3.06</sub>O<sub>10+δ</sub> Superconductors from 30 to 300 K by Positron-Lifetime Measurements. *Phys. Rev. B: Condens. Matter Phys.* 1998, 58, 15226.
- (36) Lavalley, J. C. Infrared Spectrometric Studies of the Surface Basicity of Metal Oxides and Zeolites Using Adsorbed Probe Molecules. *Catal. Today* 1996, 27, 377–401.
- (37) Di Cosimo, J.; Díez, V.; Xu, M.; Iglesia, E.; Apesteguía, C. Structure and Surface and Catalytic Properties of Mg–Al Basic Oxides. *J. Catal.* 1998, 178, 499–510.
- (38) Makwana, V. D.; Son, Y.-C.; Howell, A. R.; Suib, S. L. The Role of Lattice Oxygen in Selective Benzyl Alcohol Oxidation Using OMS-2 Catalyst: A Kinetic and Isotope-Labeling Study. *J. Catal.* 2002, 210, 46–52.
- (39) Chen, Y.; Zheng, H.; Guo, Z.; Zhou, C.; Wang, C.; Borgna, A.; Yang, Y. Pd Catalysts Supported on MnCeO<sub>x</sub> Mixed Oxides and their Catalytic Application in Solvent-Free Aerobic Oxidation of Benzyl Alcohol: Support Composition and Structure Sensitivity. *J. Catal.* 2011, 283, 34–44.
- (40) Zhao, G.; Huang, J.; Jiang, Z.; Zhang, S.; Chen, L.; Lu, Y. Microstructured Au/Ni-Fiber Catalyst for Low-Temperature Gas-Phase Alcohol Oxidation: Evidence of Ni<sub>2</sub>O<sub>3</sub>–Au<sup>+</sup> Hybrid Active Sites. *Appl. Catal., B* 2013, 140–141, 249–257.
- (41) Mondelli, C.; Ferri, D.; Grunwaldt, J. D.; Krumeich, F.; Mangold, S.; Psaro, R.; Baiker, A. Combined Liquid-Phase ATR-IR and XAS Study of the Bi-Promotion in the Aerobic Oxidation of Benzyl Alcohol over Pd/Al<sub>2</sub>O<sub>3</sub>. *J. Catal.* 2007, 252, 77–87.
- (42) Campisi, S.; Ferri, D.; Villa, A.; Wang, W.; Wang, D.; Kröcher, O.; Prati, L. Selectivity Control in Palladium-Catalyzed Alcohol Oxidation through Selective Blocking of Active Sites. *J. Phys. Chem. C* 2016, 120, 14027–14033.

- (43) Fang, W.; Chen, J.; Zhang, Q.; Deng, W.; Wang, Y. Hydrotalcite-Supported Gold Catalyst for the Oxidant-Free Dehydro-genation of Benzyl Alcohol: Studies on Support and Gold Size Effects. *Chem. - Eur. J.* 2011, 17, 1247–1256.
- (44) Feng, J.; Ma, C.; Miedziak, P. J.; Edwards, J. K.; Brett, G. L.; Li, D.; Du, Y.; Morgan, D. J.; Hutchings, G. J. Au-Pd Nanoalloys Supported on Mg-Al Mixed Metal Oxides as a Multifunctional Catalyst for Solvent-free Oxidation of Benzyl Alcohol. *Dalton T.* 2013, 42, 14498–14508.
- (45) Liu, P.; Degirmenci, V.; Hensen, E. J. Unraveling the Synergy between Gold Nanoparticles and Chromium-Hydrotalcites in Aerobic Oxidation of Alcohols. *J. Catal.* 2014, 313, 80–91.
- (46) Bates, S.; Gillan, M.; Kresse, G. Adsorption of Methanol on TiO<sub>2</sub> (110): A First-Principles Investigation. *J. Phys. Chem. B* 1998, 102, 2017–2026.
- (47) Farfán-Arribas, E.; Madix, R. J. Role of Defects in the Adsorption of Aliphatic Alcohols on the TiO<sub>2</sub> (110) Surface. *J. Phys. Chem. B* 2002, 106, 10680–10692.
- (48) Zhang, Z.; Bondarchuk, O.; White, J.; Kay, B. D.; Dohnalek, Z. Imaging Adsorbate O-H Bond Cleavage: Methanol on TiO<sub>2</sub> (110). *J. Am. Chem. Soc.* 2006, 128, 4198–4199.
- (49) Fristrup, P.; Johansen, L. B.; Christensen, C. H. Mechanistic Investigation of the Gold-Catalyzed Aerobic Oxidation of Alcohols. *Catal. Lett.* 2008, 120, 184–190.
- (50) Abad, A.; Corma, A.; García, H. Catalyst Parameters Determining Activity and Selectivity of Supported Gold Nanoparticles for the Aerobic Oxidation of Alcohols: The Molecular Reaction Mechanism. *Chem. - Eur. J.* 2008, 14, 212–222.
- (51) Yamaguchi, K.; Mizuno, N. Supported Ruthenium Catalyst for the Heterogeneous Oxidation of Alcohols with Molecular Oxygen. *Angew. Chem., Int. Ed.* 2002, 41, 4538–4542.
- (52) Sankar, M.; Nowicka, E.; Tiruvalam, R.; He, Q.; Taylor, S. H.; Kiely, C. J.; Bethell, D.; Knight, D. W.; Hutchings, G. J. Controlling the Duality of the Mechanism in Liquid-Phase Oxidation of Benzyl Alcohol Catalysed by Supported Au-Pd Nanoparticles. *Chem. - Eur. J.* 2011, 17, 6524–6532.
- (53) Delley, B. An All-Electron Numerical Method for Solving the Local Density Functional for Polyatomic Molecules. *J. Chem. Phys.* 1990, 92, 508–517.
- (54) Delley, B. From Molecules to Solids with the DMol<sup>3</sup> Approach. *J. Chem. Phys.* 2000, 113, 7756–7764.
- (55) Segall, M.; Lindan, P. J.; Probert, M. a.; Pickard, C.; Hasnip, P. J.; Clark, S.; Payne, M. First-Principles Simulation: Ideas, Illustrations and the CASTEP Code. *J. Phys.: Condens. Matter* 2002, 14, 2717– 2744.
- (56) Perdew, J. P.; Burke, K.; Ernzerhof, M. Generalized Gradient Approximation Made Simple. *Phys. Rev. Lett.* 1996, 77, 3865–3868.
- (57) Anisimov, V. I.; Zaanen, J.; Andersen, O. K. Band Theory and Mott Insulators: Hubbard U instead of Stoner I. *Phys. Rev. B: Condens. Matter Mater. Phys.* 1991, 44, 943–954.
- (58) Bajdich, M.; García-Mota, M.; Vojvodic, A.; Nørskov, J. K.; Bell, A. T. Theoretical Investigation of the Activity of Cobalt Oxides for the Electrochemical Oxidation of Water. *J. Am. Chem. Soc.* 2013, 135, 13521.
- (59) Valdes, A.; Qu, Z. W.; Kroes, G. J.; Rossmeisl, J.; Nørskov, J. K. Oxidation and Photo-Oxidation of Water on TiO<sub>2</sub> Surface. *J. Phys. Chem. C* 2008, 112, 9872–9879.